# Time-Domain Design-Oriented Parametrization of Truncated Periodic Strip Gratings

L. Carin, *Member, IEEE*, L. B. Felsen, *Life Fellow, IEEE*, and M. R. McClure, *Member, IEEE*

*Abstract*— **Asymptotic methods are used to develop an algorithm that parametrizes time-domain plane-wave interaction with a truncated grating of periodically spaced, perfectly conducting strips in free space. By distinctly displaying the edge effects as well as the truncated Floquet mode contributions from the body of the grating, the model contains the necessary building blocks for time-domain, finite-grating design. Short-pulse, plane-wave diffraction results computed from the model are shown to agree well with numerical reference data, and salient properties of the time-domain Floquet-mode constituents in the model are highlighted via time-frequency representations.**

RECENTLY, we have developed an algorithm for numerical as well as analytic-asymptotic modeling of two-dimensional time-harmonic and transient plane-wave scattering from finite gratings composed of coplanar, infinitesimally thin, perfectly conducting strips in free space [1]; the method of moments (MOM) is used to determine the currents induced on the strips. Involving edge diffractions from the ends of the grating, truncated Floquet modes from the bulk, and transition functions across Floquet-mode shadow boundaries, these constituents furnish the wave-optical tools for finite grating design. The algorithm for time-harmonic excitation has been described in a recent communication [2]; we demonstrate here corresponding results for short-pulse time-domain scattering.

The flat strips are placed in the $z = 0$ plane and the incident wave vector is oriented perpendicularly to the $y$-directed strip edges. Both TE and TM polarizations, with the electric and magnetic field vectors parallel to $y$, respectively, are considered. It was shown in [2] that, for $N$ strips, a particular component of the time-harmonic scattered field $u_s$ can be expressed approximately as

$$u_s = u_l - u_r \exp[-ik_o N d \sin\theta_i], \quad k_o = \omega/c, \qquad (1)$$

where $d$ is the period of the finite array, $\theta_i$ is the angle of incidence with respect to the $z$ axis, $c$ is the free-space propagation speed, and an $\exp[-\imath\omega t]$ time dependence has been suppressed. The asymptotically evaluated expression for $u_l$, which represents phenomena associated with the edge of the left-most unit cell, contains an edge-diffraction-like term, truncated Floquet modes, and Fresnel transition functions for the edge-induced Floquet-mode shadow boundaries. The expression $u_r$ has a similar structure with respect to the edge of the right-most unit cell. As given in [2, (4)], these expressions are inconvenient for inversion into the time domain because the shadow-boundary transition function and the contribution from a particular Floquet mode are each represented discontinuously, although their combination is continuous. This suggests replacement of each pair of discontinuous terms with a single continuous function [1], yielding

$$u_{l,r} \sim \sqrt{2\pi/\Omega_{l,r}}\, e^{\imath\Omega_{l,r}} e^{-\imath\pi/4} g(\theta_{l,r}, \theta_i) + \mathrm{sgn}(\theta_{l,r}) \sum_m i\pi a_m e^{i\Omega_{l,r}\cos[\phi_m - \theta_{l,r}]} erfc[\gamma_m], \qquad (2)$$

where $g(\theta_{l,r}, \theta_i)$ is the Floquet-mode-dependent edge-diffraction coefficient, $\Omega_{l,r} = k_o L_{l,r}$, $L_{l,r}$ are respectively the distances to the observer from the edges of the left- and right-most unit cells, $\theta_{l,r}$ are respectively the inclination angles (with respect to the $z$ axis) of rays from the edges of the left- and right-most unit cells to the observer (see Fig. 1 in [2]), $\phi_m(\omega)$ is the propagation angle and $a_m(\omega)$ the amplitude of the $m$th Floquet mode on an infinite array, erfc$(\cdot)$ denotes the error function compliment, sgn$(\cdot)$ equals 1 for positive arguments and -1 for negative arguments, and $\gamma_m = \mathrm{sgn}(\theta_{l,r})\sqrt{\Omega_{l,r}/2}\, e^{i\pi/4}(\phi_m - \theta_{l,r})$. The sum in (2) extends over all propagating Floquet modes.

The time-dependent fields $\hat{u}(x, z; t)$ corresponding to the time-harmonic fields $u_s(x, z; \omega)$ are related as follows:

$$\hat{u_s}(x, z; t) = \frac{1}{2\pi} \int_{-\infty}^{\infty} u_s(x, z; \omega) F(\omega) e^{-\imath\omega t} d\omega$$

$$F(\omega) = \int_{-\infty}^{\infty} f(t) e^{\imath\omega t} dt, \qquad (3)$$

where $f(t)$ is the temporal behavior of the incident waveform. The approximate asymptotic expressions in (1) and (2) will be used for $u_s(x, z; \omega)$ such that the time-domain asymptotics can be interpreted in terms of wavefronts emanating from the edges of the array and time-domain Floquet modes from the bulk.

The phase $\Omega_{l,r}$ for the edge-diffraction-like (first) term in (2) is nondispersive and therefore not amenable to saddle-point asymptotics; we have inverted this contribution numerically by FFT from the frequency domain. With regard to the asymptotic inversion of the Floquet-mode terms in (2), the functions $a_m$ and erfc are treated as amplitude terms. In

Manuscript received November 23, 1992. This work was supported in part by the Office of Naval Technology under Contract N6601–91–C06018, by the National Science Foundation under Grant ECS-9211353, and by the Air Force Office of Scientific Research under Grant F49620–93–1–0093.

L. Carin and L. B. Felson are with the Department of Electrical Engineering/Weber Research Institute, Polytechnic University, Brooklyn, NY 11201.

M. R. McClure is with the Missile Systems Division, Raytheon Company, Tewksbury, MA 01876.

IEEE Log Number 9207949.

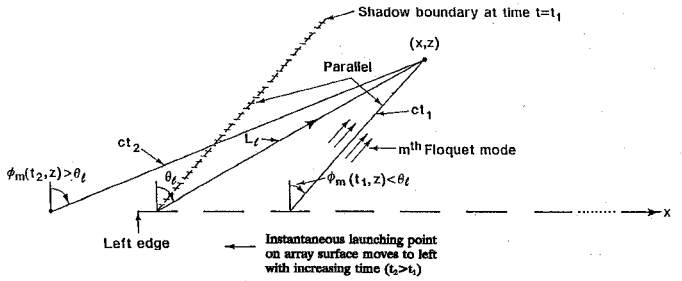


Fig. 1. Schematization of TD $m$th Floquet behavior with respect to left edge of truncated array. The angle $\phi_m(t,z)$ tags the propagation direction of the $m$th Floquet mode with local frequency $\bar{\omega}_m(t)$ away from the array surface. For $\phi_m < \theta_l$, the mode contributes to the scattered field, but it does not contribute for $\phi_m > \theta_l$. The local region, where the scattered field originates on the array, moves to the left with increasing time. Instantaneous shadow boundary of the $m$th Floquet mode is also shown.

rectangular coordinates, the phase of the $m$th Floquet mode becomes $\Psi_m(x,z;\omega,t) = k_{xm}(\omega)x + k_{zm}(\omega)z - \omega t$ , with $k_{xm}(\omega) = (2m\pi/d) - k_o \sin\theta_i$ and $k_{zm} = \sqrt{k_o^2 - k_{xm}^2}$ . Restricting to normal incidence ($\theta_i = 0$) for simplicity, the $m = 0$ Floquet mode also has a nondispersive phase and is therefore converted to the time domain via the FFT. All higher order propagating Floquet modes ($m \neq 0$) have a nonlinear frequency dependence in the phase and can be evaluated approximately via saddle-point asymptotics. It is easily verified that the saddle-point frequencies $\bar{\omega}_m$ defined by $\partial\Psi_m/\partial\omega = 0$ are given explicitly by

$$\bar{\omega}_m(z,t) = \pm\frac{c\tau 2\pi|m|}{d\sqrt{\tau^2 - z^2}}, \qquad m \neq 0, \qquad \theta_i = 0, \qquad (4)$$

where $\tau = ct$ . After the saddle points have been determined, the asymptotic saddle-point approximation [3] for the time-domain truncated $m \neq 1$ Floquet modes are computed easily [1]. The interpretation of the time-domain results, however, can be carried out directly from the saddle-point condition (4) and Fig. 1.

Recalling that, for normal incidence, the frequency-dependent propagation angle of the $m$th Floquet mode on an infinite array satisfies $\sin\phi_m(\omega) = 2m\pi c/\omega d$, one finds that the angle of propagation $\phi_m(z,t)$ of the $m$th Floquet mode at time $t$ with saddle point $\bar{\omega}_m(z,t)$ satisfies $\sin\phi_m(z,t) = \sqrt{1-(z/\tau)^2}$ . Thus, the fields at a given relative time $t$ can be attributed to scattering from that particular location on the truncated array which has a signal transit time $t$ to the observer (Fig. 1). Note that the angle $\phi_m(z,t)$ is independent of $m$ and is therefore the same for all Floquet modes, and that the saddle-point frequency $\bar{\omega}_m(z,t)$ increases with modal index $m$ but decreases with increasing time $t$ (approaching the cutoff wavelength $\lambda_{cm} = d/m$ of the $m$th Floquet modes as $t \to \infty$). Moreover, due to the finite bandwidth of the incident waveform, only a finite number of Floquet modes will contribute to the scattered field, each with its own unique time-dependent frequency.

As depicted in Fig. 1, for the $m$th Floquet mode, the angle $\phi(z,t)$ increases with time until it approaches $\theta_l$. For $\phi(z,t) > \theta_l$, the asymptotic evaluation shows that the Floquet modes no longer contribute to the scattered field. Similar phenomena are associated with the right edge of the truncated array. In addition to the contributions from the higher order Floquet modes previoulsy discussed, the total time-dependent field also includes contributions from the $m = 0$ mode and from edge diffraction originating at the ends of the truncated array. In the time domain, each represents a waveform that propagates without dispersion, appropriately delayed with respect to its scattering center.

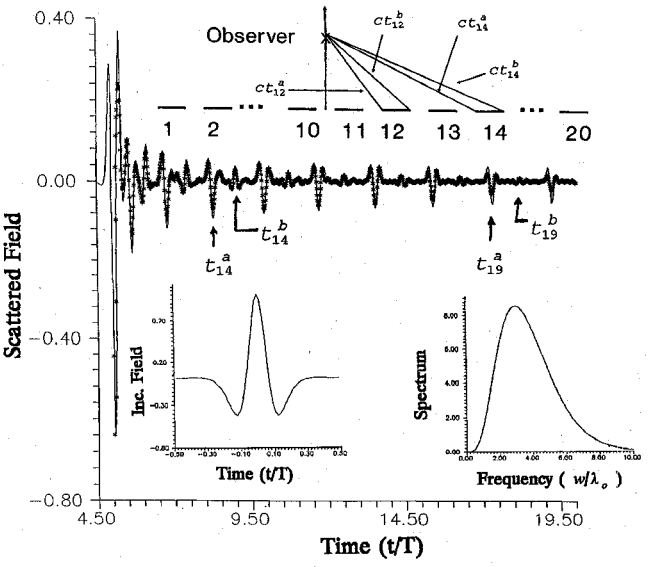


Fig. 2. Time-domain scattered field due to a pulsed plane wave incident normally on a planar grating composed of 20 infinitesimally thin, perfectly conducting strips of width and interstrip spacing $w$. Field is observed $5w$ directly above the array center. Dots represent results calculated by summing the asymptotically approximated TD Floquet modes with order $1 \leq |m| \leq 10$, which cover the frequency range of the pulse spectrum. Curve represents the results of a reference MOM-FFT algorithm. Arrows identify pulse arrivals and their points of origin on the array. Time and frequency dependence of the incident waveform are also shown. The time is normalized to $T$, where $T = w/c$.

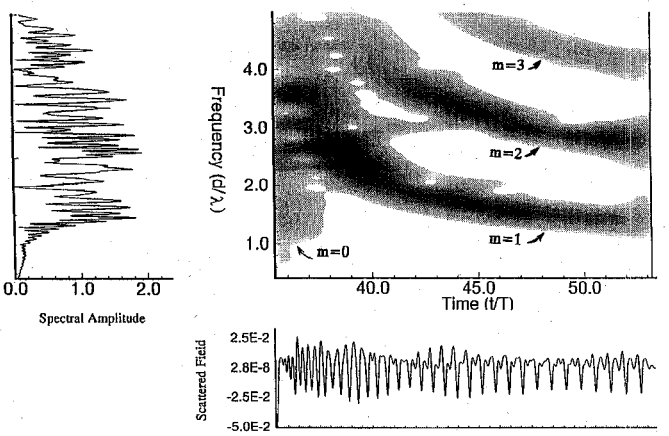


Fig. 3. Time-frequency representation for scattered field due to a pulsed plane wave incident normally upon a forty-strip grating. The grating period is $d$, the strip width is 0.06 $d$, and the interstrip separation is 0.94 $d$. The scattered fields are observed at 35.44 $d$ directly above the right-most edge of the array. The TD waveform (bottom) was computed using a MOM–FFT reference algorithm. The left-most figure is a Fourier transform of the entire TD waveform. Center figure was computed by performing on the TD waveform a short-time Fourier transform (STFT) with a Gaussian window having $\sigma/T = 1.2$. Time is normalized to $T$, where $T = d/c$.

Consider a pulsed plane wave incident normally on a 20-strip planar grating composed of infinitesimally thin, perfectly

conducting strips of width and interstrip spacing $w$; the field observed 5 $w$ directly above the array center is plotted in Fig. 2. The dots represent results calculated by summing the saddle-point approximations for the time-domain Floquet modes with order $1 \leq |m| \leq 10$, which cover the frequency range of the pulse spectrum. Contributions from the $m = 0$ time-domain Floquet mode and from time-domain edge-diffracted fields have not been included. The dispersionless contribution from the $m = 0$ mode affects only the early (specular) return, and the edge diffraction terms contribute minimally to the observed signal at observation points in the Floquet-mode illuminated region of the grating.

To illustrate how to extract the time-dependent Floquet-mode frequencies from high-resolution short-pulse data, we consider a 40-strip array with period $d$ such that $d/\lambda_{\text{cent}} = 2.5$, where the wavelength $\lambda_{\text{cent}}$ corresponds to the center frequency of the incident waveform. With this incident-pulse bandwidth, only three higher order Floquet modes are excited. As in the solid curve of Fig. 2, the time-domain scattered field was computed by an FFT reference code. A time-frequency distribution for the scattered signal, obtained by applying to the scattered field a short-time Fourier transform with a Gaussian window [4], is shown in Fig. 3. In the early time, the specular reflection due to the dispersionless $m = 0$ mode contains the entire frequency content of the incident waveform. As time evolves, one clearly sees the distinct Floquet modes emerge with their time-dependent frequencies, which tend toward the cutoff frequencies $d/\lambda_m = m$ for the $m = 1, 2$, and 3 modes.

The results presented here demonstrate the utility of the algorithm for calculating and physically interpreting the time-domain scattered fields from a finite periodic strip grating. The synthesizing time-domain finite-aperture Floquet modes, with their time-dependent frequencies, should prove useful in the design of finite gratings for time-domain applications.

## REFERENCES

[1] L. Carin and L. B. Felsen, "Time-harmonic and transient scattering by finite periodic flat strip arrays; hybrid (ray)-(Floquet mode)-(MOM) algorithm and its GTD interpretation," to appear in *IEEE Trans. Antennas Propagat.*, Apr. 1993.

[2] ——, "Design-oriented parametrization of truncated periodic-strip gratings," *IEEE Microwave Guided Wave Lett.*, vol. 2, pp. 367–369, Sept. 1992

[3] L. B. Felsen and N. Marcuvitz, *Radiation and Scattering of Waves.* Englewood Cliffs, NJ: Prentice Hall, 1973.

[4] A. Moghaddar and E. K. Walton, "Time-frequency-distribution analysis of dispersive targets," presented at the *Workshop on High-Frequency Electromagnetic Modeling of Jet Engine Cavities*, Wright Laboratory, Wright-Patterson AFB, OH, Aug. 1–2, 1991.